



# HHS Public Access

Author manuscript

*J Mech Phys Solids*. Author manuscript; available in PMC 2019 November 01.

Published in final edited form as:

*J Mech Phys Solids*. 2018 November ; 120: 199–207. doi:10.1016/j.jmps.2017.11.002.

## The equivalent medium of cellular substrate under large stretching, with applications to stretchable electronics

Hang Chen<sup>a,b,d,1</sup>, Feng Zhu<sup>c,d,1</sup>, Kyung-In Jang<sup>e</sup>, Xue Feng<sup>a</sup>, John A. Rogers<sup>f</sup>, Yihui Zhang<sup>a</sup>, Yonggang Huang<sup>d,\*</sup>, and Yinji Ma<sup>a,d,\*</sup>

<sup>a</sup>Department of Engineering Mechanics; Center for Mechanics and Materials, Tsinghua University, Beijing, 100084, China

<sup>b</sup>Guangzhou Institute of Building Science, Technology Development Center, China, 510440, China

<sup>c</sup>School of Logistics Engineering, Wuhan University of Technology, Wuhan, China

<sup>d</sup>Departments of Civil and Environmental Engineering, Mechanical Engineering, and Materials Science and Engineering; Center for Bio-Integrated Electronics, Northwestern University, Evanston, IL 60208, USA

<sup>e</sup>Department of Robotics Engineering, Daegu Gyeongbuk Institute of Science and Technology (DGIST), Daegu 42988, South Korea

<sup>f</sup>Departments of Materials Science and Engineering, Biomedical Engineering, Chemistry, Mechanical Engineering, Electrical Engineering and Computer Science; Center for Bio-Integrated Electronics; Simpson Querrey Institute for Nano/biotechnology; Northwestern University, Evanston, Illinois 60208, USA

### Abstract

The concepts of open, cellular substrates for stretchable electronic systems are of interest partly due to their ability to minimize disruptions to the natural diffusive or convective flow of bio-fluids in advanced, bio-integrated implants. The overall elastic properties, and in particular the stretchability, of such systems are difficult to determine, however, because they depend strongly on the alignment and position of the serpentine interconnects relative to the openings in the cellular substrate, which is difficult to precisely control, even with the assistance of precision stages and visualization hardware. This paper establishes an analytic constitutive model for an equivalent medium for a cellular substrate under finite deformation. Results demonstrate that the elastic stretchability of a serpentine interconnect bonded to this equivalent medium represents a lower-bound estimate for the case of the actual cellular substrate, where the bonding adopts different alignments and positions. This finding provides a simple, conservative estimate of stretchability,

\*To whom correspondence may be addressed: y-huang@northwestern.edu (Y. Huang), mayinji@gmail.com (Y. Ma).

<sup>1</sup>These authors contributed equally to this work.

**Publisher's Disclaimer:** This is a PDF file of an unedited manuscript that has been accepted for publication. As a service to our customers we are providing this early version of the manuscript. The manuscript will undergo copyediting, typesetting, and review of the resulting proof before it is published in its final citable form. Please note that during the production process errors may be discovered which could affect the content, and all legal disclaimers that apply to the journal pertain.

which has general utility as an engineering design rule for platforms that exploit cellular substrates in stretchable electronics.

## Keywords

equivalent medium for cellular materials; constitutive model under finite deformation; stretchable electronics; elastic stretchability

---

## 1. Introduction

Recent progress in advanced materials and mechanics design concepts has led to rapid development of diverse types of stretchable electronics technologies in which high performance inorganic electronic materials are exploited to yield systems with impressive levels of mechanical flexibility and stretchability, for wide range of biological and medical applications from eye-like digital cameras (Ko et al., 2008), to devices that integrate with or deploy inside blood vessels (Klinker et al., 2015; Lee et al., 2015) to circuits that softly laminate onto brain (Kang et al., 2016; Zhang et al., 2016), heart (Lu et al., 2015; Xu et al., 2015) and skin (Jang et al., 2016; Koh et al., 2016; Li et al., 2017b; Webb et al., 2015). The fundamental approach is to exploit deformable interconnects to isolate brittle materials from strains associated with overall system deformation, thereby allowing complex combinations of stretching, bending and twisting without fracture or degradation in properties (Avila and Xue, 2017; Chen et al., 2016a; Chen et al., 2016b; Yang et al., 2017).

Significant efforts have been devoted to designs in stretchable devices (Rogers et al., 2010). The most common approach is for all functional components to reside on rigid device “islands” that are electrically and mechanically linked by stretchable/deformable interconnects (Choi et al., 2016; Lu and Yang, 2015; Ma et al., 2017; Song, 2015; Zhang et al., 2015). These interconnects can either adopt an out-of-plane arc shape formed by buckling due to release of substrate pre-strain (Jones et al., 2004; Khang et al., 2006; Lacour et al., 2005; Ma et al., 2016b; Su et al., 2012; Wang et al., 2017), or an in-plane serpentine shape (Gonzalez et al., 2008; Huyghe et al., 2008; Liu and Lu, 2016; Xu et al., 2017; Zhang and Parnell, 2017), to achieve stretchability at the system level. Such systems with islands and interconnects are always integrated on or encapsulated into solid substrates that support and protect the systems when mounted on biological tissues (Li et al., 2017a).

A disadvantages of such an approach is that this type of solid substrate/encapsulation disrupts the natural diffusive or convective flows of bio-fluids (Dou et al., 2015) through the stretchable electronics. Lee et al. (Lee et al., 2017) proposed a bio-inspired honeycomb cellular substrate to achieve high permeability as a solution to this problem. In addition, the cellular substrate has much lower equivalent modulus than a solid substrate made of the same material (Jang et al., 2015), thereby allowing it to achieve much larger stretchability, as discussed in the following.

Stretchability is one of the most important defining properties of such classes of electronics, where the values range from ~30% for epidermal applications (Kim et al., 2011b) and multifunctional integumentary membranes for cardiac measurements and stimulation (Xu et

al., 2014; Xu et al., 2015), to ~125% for catheter-based devices for cardiac ablation therapy (Kim et al., 2011a). One major challenge with stretchable electronics that exploit cellular substrates is the difficulty associated with precisely positioning the interconnects and other features of the electronics relative to the cellular substrates. Consequently, the degree of stretchability of the integrated systems cannot be accurately determined because, as shown in this paper, the stretchability depends on the alignment and position of interconnects. This paper aims to establish the lower-bound estimates of the stretchability with respect to all alignments and positions of a representative interconnect on cellular substrate. An analytic constitutive model for the equivalent medium of the cellular substrate under finite deformation is established in Section 2, which agrees well with direct numerical simulations even at 100% applied strain. Section 3 compares the elastic stretchability of the serpentine interconnect bonded to the equivalent medium to that bonded to the cellular substrate with 32 different alignments, positions and directions. It is shown that the elastic stretchability for the equivalent medium is a lower bound of that for the cellular substrate with different alignments. The resulting values represent a simple, conservative estimate of the elastic stretchability, and is useful to the design of stretchable electronics bonded to cellular substrate.

It should be pointed out that there exist extensive studies on mechanics of the cellular structure under infinitesimal deformation (e.g., Chen et al., 2016c; Giboson and Ashby, 1997; Giboson et al., 1982; Hasanyan and Waas, 2016; Mora and Waas, 2007; Okumura et al., 2004; Zhu, 2010), and few studies under finite deformation based on the neo-Hookean constitutive model (e.g., Mihai and Goriely, 2015; Mihai et al., 2017) For stretching beyond 20%, the neo-Hookean models deviate substantially from the direct numerical simulations, therefore fall short for applications to stretchable electronics involving very large stretching (e.g., 100%).

## 2. An analytic, constitutive model of a cellular substrate under finite deformation

Let  $E_0$  denote the linear elastic modulus of the cell walls. In general, the relation between the nominal stress and engineering strain of the virgin material for the cellular walls can be written as  $\sigma = E_0 f(\epsilon)$ , where the function  $f$  satisfies  $df/d\epsilon|_{\epsilon=0} = 1$ . This section aims to establish the stress-strain relation of the equivalent medium for the cellular substrate in terms of  $f$  and the porosity  $\phi$  of the cellular substrate.

The cellular substrate used in stretchable electronics has high porosity (> 70%) (Lee et al., 2017) to offer both high permeability and stretchability. Figure 1a shows a schematic illustration of the hexagonal cellular substrate with the (center-to-center) cell size  $d$ . The cell walls have length  $l = d/\sqrt{3}$  and width  $\delta = d(1 - \sqrt{\phi})$ . For a high porosity such as 80% as in experiments (Lee et al., 2017), the cell wall width  $\delta$  is much smaller than its length  $l$  such that cell walls can be modeled as beams. For uniaxial stretching along the  $x$ -direction of the global coordinate system  $\{x, y\}$  (parallel to the cell wall), the basic unit for the cellular substrate, as shown in Fig. 1b, consists of three beams of length  $l/2$  and  $120^\circ$  apart. Let  $2P$  denote the force (per unit thickness along the out-of-plane direction) in the cell wall along  $x$ -

direction (Fig. 1b), which gives the nominal stress in this wall, normalized by  $E_0$ , as  $\hat{T}_h = 2P/(E_0\delta) = \hat{T}/(1 - \sqrt{\phi})$ , where  $\hat{T} = 2P/(E_0 d)$  is the nominal stress in the equivalent medium of the cellular substrate, also normalized by  $E_0$ . From the uniaxial stress-strain curve  $\sigma = E_0 f(\epsilon)$  of the virgin material for the cell walls, the engineering strain in the cell walls parallel to the stretching direction is

$$\epsilon_h = f^{-1}(\hat{T}_h) = f^{-1}\left(\frac{\hat{T}}{1 - \sqrt{\phi}}\right). \quad (1)$$

Finite element analysis (Lee et al., 2017) shows that the strains in the inclined cell walls (not parallel to the stretching direction  $x$ ) are much smaller than the strain along the  $x$  direction. Therefore, the linear elastic relation is used for the inclined cellular walls. A local coordinate system  $\{\bar{x}, \bar{y}\}$  is introduced with  $\bar{x}$  axis parallel to an inclined cellular wall, as shown in Figs. 1b and 2. Let  $S$  and  $s$  denote the arc length along the axis of the inclined cellular wall before and after the deformation, respectively, and  $\varphi = \varphi(s)$  the angle between the tangent and the  $\bar{x}$  axis (Fig. 2). The shear force  $Q$  and axial force  $N$  in the inclined cellular wall (Fig. 2) are related to  $P$  and  $\varphi$  as

$$N = P \cos(\pi/3 - \varphi), \quad (2a)$$

$$Q = -P \sin(\pi/3 - \varphi). \quad (2b)$$

Equilibrium of force in the inclined wall gives (Ma et al., 2016a; Ma and Zhang, 2016)

$$\frac{dQ}{ds} - N \frac{d\varphi}{ds} = 0, \text{ or } \frac{dQ}{dS} - N \frac{d\varphi}{dS} = 0, \quad (3a)$$

$$\frac{dN}{ds} + Q \frac{d\varphi}{ds} = 0, \text{ or } \frac{dN}{dS} + Q \frac{d\varphi}{dS} = 0, \quad (3b)$$

where  $ds$  and  $dS$  are related to the strain  $N/(E_0\delta)$  in the inclined wall by  $ds/dS = 1 + N/(E_0\delta)$  (Fan et al., 2017). Equilibrium of moment  $M$  in the inclined wall (Fig. 2) gives

$$Q = \frac{dM}{ds}, \text{ or } \left(1 + \frac{N}{E_0\delta}\right) Q = \frac{dM}{dS}. \quad (3c)$$

Substitution of Eq. (2) into the moment equilibrium in Eq. (3c), together with the moment-curvature relation  $M = E_0 I d\varphi/dS$  (Ma et al., 2016a), give

$$\frac{d^2\varphi}{dS^2} = -\frac{P}{E_0 J} \left[ \sin\left(\frac{\pi}{3} - \varphi\right) + \frac{1}{2E_0\delta} P \sin\left(\frac{2\pi}{3} - 2\varphi\right) \right], \quad (4)$$

where  $E_0 I = E_0 \delta^3/12$  is the bending stiffness of cellular walls. The above equation, together with  $\hat{T} = 2P/(E_0 d)$ ,  $\delta = d(1 - \sqrt{\phi})$  and the moment free condition  $(d\varphi/dS)|_{S=l/2}$  due to symmetry, give

$$\left(\frac{d\varphi}{dS}\right)^2 = \frac{12\hat{T}}{(1 - \sqrt{\phi})^3 d^2} \left\{ \cos\left(\frac{\pi}{3} - \varphi\right) - \cos\beta + \frac{\hat{T}}{8(1 - \sqrt{\phi})} \left[ \cos\left(\frac{2\pi}{3} - 2\varphi\right) - \cos 2\beta \right] \right\}, \quad (5)$$

where  $\beta = \pi/3 - \varphi|_{s=l/2} = \pi/3 - \varphi|_{s=\sqrt{3}d/6}$  is determined from the following equation obtained by integrating Eq. (5) from  $S = 0$  to  $S = l/2$ , i.e.,

$$\int_0^{\pi/3 - \beta} \frac{d\varphi}{\sqrt{\left\{ \cos\left(\frac{\pi}{3} - \varphi\right) - \cos\beta + \frac{\hat{T}}{8(1 - \sqrt{\phi})} \left[ \cos\left(\frac{2\pi}{3} - 2\varphi\right) - \cos 2\beta \right] \right\}}} = \sqrt{\frac{\hat{T}}{(1 - \sqrt{\phi})^3}}, \quad (6)$$

which gives  $\beta$  in terms of the porosity  $\phi$  and normalized nominal stress  $\bar{T}$ . The local coordinates of the end of the inclined wall (Point B in Figs. 1b and 2) can be obtained from  $\varphi$  in Eq. (5), and  $d\bar{x}/ds = \cos\varphi$  and  $d\bar{y}/ds = \sin\varphi$ , as

$$\begin{aligned} \begin{Bmatrix} \hat{x}_{B\_end} \\ \hat{y}_{B\_end} \end{Bmatrix} &\equiv \frac{1}{d} \begin{Bmatrix} \bar{x}_{B\_end} \\ \bar{y}_{B\_end} \end{Bmatrix} \\ &= \int_0^{\pi/3 - \beta} \frac{\begin{Bmatrix} 1 + \frac{\hat{T}\cos(\pi/3 - \varphi)}{2(1 - \sqrt{\phi})} \\ \sin\varphi \end{Bmatrix} d\varphi}{2\sqrt{\frac{3\hat{T}}{(1 - \sqrt{\phi})^3} \left\{ \cos(\pi/3 - \varphi) - \cos\beta + \frac{\hat{T}}{8(1 - \sqrt{\phi})} [\cos(2\pi/3 - 2\varphi) - \cos 2\beta] \right\}}}. \end{aligned} \quad (7)$$

The global coordinates  $\{x, y\}$  of the end of the inclined wall, normalized by  $d$ , are obtained as

$$\begin{Bmatrix} \hat{x}_{B\_end} \\ \hat{y}_{B\_end} \end{Bmatrix} = \begin{Bmatrix} \cos\frac{\pi}{3} & \sin\frac{\pi}{3} \\ -\sin\frac{\pi}{3} & \cos\frac{\pi}{3} \end{Bmatrix} \begin{Bmatrix} \hat{x}_{B\_end} \\ \hat{y}_{B\_end} \end{Bmatrix}. \quad (8)$$

Equation 1 gives the coordinates  $\{x, y\}$  (normalized by  $d$ ) of the end of the cellular wall parallel to the stretching direction (Point A in Fig. 1a) as

$$\hat{x}_{A\_end} = -\frac{1}{2\sqrt{3}} \left[ 1 + f^{-1} \left( \frac{\hat{T}}{1 - \sqrt{\phi}} \right) \right], \quad (9a)$$

$$\hat{y}_{A\_end} = 0. \quad (9b)$$

Equations 8 and 9, together with the initial coordinates ( $\hat{x}_{B\_end} |_{\hat{T}=0} = 1/4\sqrt{3}$ ,  $\hat{y}_{B\_end} |_{\hat{T}=0} = -1/4$ ,  $\hat{x}_{A\_end} |_{\hat{T}=0} = 1/2\sqrt{3}$ ,  $\hat{y}_{A\_end} |_{\hat{T}=0} = 0$ ), give the equivalent engineering strains of the cellular substrate parallel and perpendicular to the stretching direction ( $x$ - and  $y$ -direction, respectively) as

$$\varepsilon_{x\_cellular} \equiv \frac{\hat{x}_{B\_end} - \hat{x}_{A\_end}}{\hat{x}_{B\_end} |_{\hat{T}=0} - \hat{x}_{A\_end} |_{\hat{T}=0}} = \frac{4(\hat{x}_{B\_end} - \hat{x}_{A\_end})}{\sqrt{3}}, \quad (10a)$$

$$\varepsilon_{y\_cellular} \equiv \frac{\hat{y}_{B\_end} - \hat{y}_{A\_end}}{\hat{y}_{B\_end} |_{\hat{T}=0} - \hat{y}_{A\_end} |_{\hat{T}=0}} = -4\hat{y}_{B\_end}, \quad (10b)$$

where  $\hat{x}_{A\_end}$ ,  $\hat{x}_{B\_end}$  and  $\hat{y}_{B\_end}$  are obtained from Eqs. 7, 8 and 9, and they depend on the porosity  $\phi$ , normalized nominal stress  $\hat{T}$  and uniaxial stress-strain curve  $\sigma = E_0 f(\varepsilon)$  of the virgin material. The equivalent Poisson's ratio of the cellular substrate is defined from the increments of  $\varepsilon_{x\_cellular}$  and  $\varepsilon_{y\_cellular}$  as

$$\nu_{cellular} \equiv \frac{d\varepsilon_{y\_cellular}}{d\varepsilon_{x\_cellular}} = -\frac{d\varepsilon_{y\_cellular}/d\hat{T}}{d\varepsilon_{x\_cellular}/d\hat{T}}, \quad (11)$$

where  $d\varepsilon_{x\_cellular}/d\hat{T}$  and  $d\varepsilon_{y\_cellular}/d\hat{T}$  are obtained from Eq. 10.

The incompressible Mooney-Rivlin constitutive relation (Mooney, 1940) is adopted in the following to illustrate the analytic constitutive model above. It gives analytically the uniaxial stress-strain curve  $\sigma = E_0 f(\varepsilon)$ , where  $f(\varepsilon)$  is given by

$$f(\varepsilon) = \frac{1}{15} \left( 4 + \frac{1}{1 + \varepsilon} \right) \left[ 1 + \varepsilon - \frac{1}{(1 + \varepsilon)^2} \right], \quad (12)$$

and the only material property is the linear elastic modulus  $E_0$ . Equations (10a) and (11) then give the nominal stress (normalized by  $E_0$ ) and Poisson's ratio of the equivalent medium of the cellular substrate, which are shown versus the engineering strain (up to

100%) in Figs. 3a and b, respectively, at different high porosities ( $\phi = 50\%$ , 60%, 70%, 80% and 90%). Figures 3a and b also show the stress-strain curve and Poisson's ratio of the cellular substrate directly obtained from finite element analysis (FEA). It is clear that, for  $\phi = 50\%$ , the analytic constitutive model for the equivalent medium of the cellular substrate agrees well with the numerical results without any parameter fitting.

The stress-strain curves are obtained by FEA for the cellular substrates stretched along  $x$ -,  $45^\circ$  and  $y$ -directions, as shown in Fig. 4a. The incompressible Mooney-Rivlin constitutive model is used for the cellular walls. The normalized stress-strain curves of the equivalent medium for the cellular substrate are shown in Fig. 4b. At each porosity ranging from  $\phi = 50\%$  to 90%, the normalized stress-strain curves are essentially the same for stretching along different directions. Therefore, the equivalent medium for the cellular substrate can be approximated as isotropic, and the analytic model above derived for stretching along the cell wall direction is applicable for any direction.

### 3. Stretchability of serpentine interconnect on a cellular substrate

For a serpentine interconnect bonded to a cellular substrate, FEA can define the stretchability for three representative shapes that have the same width ( $w = 50 \mu\text{m}$ ), same cross section [0.1  $\mu\text{m}$ -thick Cu (elastic modulus 119 GPa, Poisson's ratio 0.34) sandwiched by two 1.2  $\mu\text{m}$ -thick layers of PI (elastic modulus 2.5 GPa, Poisson's ratio 0.34)], same radius  $R = \sqrt{3}d/2 = 0.45 \text{ mm}$  for the circular part but different lengths  $L$  [1.04 mm (Figs. 5a and d), 0.52 mm (Figs. 5b and e) and 0 (Figs. 5c and f), respectively] of the straight part of the serpentine interconnect, as in Fig. 5. The cellular substrate consists of a 0.35 mm thick layer of PDMS with a porosity  $\phi = 80\%$  and cell size  $d = 0.52 \text{ mm}$ , where the elastic modulus and Poisson's ratio of PDMS are 500 kPa and 0.5 (Lee et al., 2017), respectively.

In practice, it can be difficult to precisely control the alignment and position of the serpentine interconnect on the cellular substrate. Finite element analysis is used to study the stretchability of three representative shapes of serpentine interconnects in Fig. 5, which are bonded to the cellular substrate along  $x$ - (Figs. 5a-c) and  $y$ -directions (Figs. 5d-f). For each shape and each direction of the serpentine interconnect, 16 alignments with all combinations of offset by 0,  $\sqrt{3}d/6$ ,  $\sqrt{3}d/3$  and  $\sqrt{3}d/2$  along  $x$ -direction (parallel to cell wall, Fig. 5), and 0,  $d/6$ ,  $d/3$  and  $d/2$  along  $y$ -direction (perpendicular to cell wall) are studied. The elastic stretchability, defined for 0.3% yield strain of Cu, has a large variation among all 32 alignments for each shape in Fig. 5. For the serpentine interconnect with long straight part  $L = 1.04 \text{ mm}$  (Figs. 5a and d), the mean elastic stretchability is 85% for all 32 alignments, with the standard deviation 18%. For the serpentine interconnects with medium straight part  $L = 0.52 \text{ mm}$  (Figs. 5b and e) and no straight part  $L = 0$  (Figs. 5c and f), the mean elastic stretchabilities are 74% and 45%, with the standard deviations 13% and 4%, respectively. It is clear that the elastic stretchability increases with the length of the straight part of serpentine interconnect.

Finite element analysis is also used to study the elastic stretchability of serpentine interconnect bonded to a solid substrate, which has the analytic constitutive model in Section 2 for the equivalent medium of the cellular substrate with porosity  $\phi = 80\%$ . For three shapes

of the serpentine interconnect in Fig. 5, the elastic stretchabilities are 73%, 65% and 34%, respectively, which are the lower bound of the elastic stretchabilities obtained for 32 alignments and directions discussed above, as shown in Fig. 6. This is because the cellular substrate allows the serpentine interconnect to buckle freely in the open space, while the equivalent medium, even though it has a low elastic modulus, still constraints the serpentine interconnect. Therefore, the equivalent medium in Section 2 yields an effective way to estimate the lower bound of elastic stretchability of the serpentine interconnect bonded to a cellular substrate. This lower-bound estimate is useful to design stretchable electronics on cellular substrate without the need to accurately determine the alignment.

In the following the substrate is fixed as a 0.35 mm-thick solid, equivalent medium for cellular PDMS with porosity  $\phi = 80\%$ . The cross-section thicknesses and materials (1.2  $\mu\text{m}$ -thick PI/ 0.1  $\mu\text{m}$ -thick Cu/ 1.2  $\mu\text{m}$ -thick PI) of the serpentine interconnect are also fixed in order to study effects of width  $w$  and length  $L$  of the straight part. Figure 6 shows the elastic stretchability versus the width  $w$  for the length of straight part  $L = 1.04$  mm and the radius  $R = \sqrt{3}d/2 = 0.45$  mm of circular part of the serpentine interconnect. A narrow serpentine interconnect ( $w = 50$   $\mu\text{m}$ ) yields significantly larger stretchability than those for wider ones ( $w$  from 75  $\mu\text{m}$  to 175  $\mu\text{m}$ ). This is because, for wide serpentine interconnects, the outer edge of the arc wrinkles with large amplitude when under stretching, as shown in the inset in Fig. 7, which leads to a large local strain in Cu, therefore a low elastic stretchability.

Figure 6 suggests that the elastic stretchability increases with length  $L$  of the straight part of serpentine interconnect, but this increase saturates as  $L$  reaches approximately twice the radius  $R$  of the circular part. With the width  $w = 50$   $\mu\text{m}$  (as suggested by Fig. 7), the elastic stretchability of serpentine interconnect on the solid, equivalent medium of the cellular substrate is shown versus the length-to-radius ratio  $L/R$  in Fig. 8 for two radii  $R = 0.45$  mm and 0.25 mm. The elastic stretchability clearly increases with the radius  $R$  because, for small radius, the outer edge of the arc also wrinkles with large amplitude when under stretching, as shown in the inset in Fig. 8, therefore a low elastic stretchability. The elastic stretchability increases with  $L/R$ , and saturates once  $L/R = \sim 2$ , which is the suggested ratio for the design of serpentine interconnect.

#### 4. Concluding remarks

1. An analytic constitutive model is established for an equivalent medium for a cellular substrate under finite deformation. For porosity  $\phi = 50\%$ , the effective properties (e.g., nonlinear stress-strain relation under finite deformation, Poisson's ratio) of the equivalent medium predicted by this analytic constitutive model agree well with those of the cellular substrate, without any parameter fitting.
2. The elastic stretchability of the serpentine interconnect bonded to the equivalent medium is a lower-bound estimate of that bonded to the cellular substrate. This lower-bound estimate is important to the design of stretchable electronics that use cellular substrates because its stretchability depends strongly on the



alignment and position of interconnects on the cellular substrate, which are difficult to precisely control.

## Acknowledgments

H.C. acknowledges the support from the National Natural Science Foundation of China (Grants Nos. 51608139 and 51678171) and China Postdoctoral Science Foundation (Grant No. 2016M592471). F.Z. acknowledges the support from the China Scholarship Council. K.-I. J. acknowledges the support from the National Research Foundation of Korea (NRF-2017M3A7B4049466). X.F. acknowledges the support from the National Basic Research Program of China (Grant No. 2015CB351900) and the National Natural Science Foundation of China (Grant No. 11320101001). Y.H. acknowledges the support from NSF (Grant Nos. CMMI1400169 and CMMI1534120) and NIH (Grant No. R01EB019337). Y.M. acknowledges the support from the National Natural Science Foundation of China (Grant No. 11402135).

## References

- Avila R, Xue Y. Torsional Buckling by Joining Prestrained and Unstrained Elastomeric Strips With Application as Bilinear Elastic Spring. *J Appl Mech-T ASME*. 2017; 84:104502.
- Chen YL, Liu YL, Yan Y, Zhu Y, Chen X. Helical coil buckling mechanism for a stiff nanowire on an elastomeric substrate. *J Mech Phys Solids*. 2016a; 95:25–43.
- Chen YL, Zhu Y, Chen X, Liu YL. Mechanism of the Transition From In-Plane Buckling to Helical Buckling for a Stiff Nanowire on an Elastomeric Substrate. *J Appl Mech-T ASME*. 2016b; 83:041011.
- Chen YM, Das R, Battley M. Response of Honeycombs Subjected to In-Plane Shear. *J Appl Mech-T ASME*. 2016c; 83:061004.
- Choi S, Lee H, Ghaffari R, Hyeon T, Kim DH. Recent Advances in Flexible and Stretchable Bio-Electronic Devices Integrated with Nanomaterials. *Adv Mater*. 2016; 28:4203–4218. [PubMed: 26779680]
- Dou YY, Jin ML, Zhou GF, Shui LL. Breath Figure Method for Construction of Honeycomb Films. *Membranes*. 2015; 5:399–424. [PubMed: 26343734]
- Fan ZC, Wu J, Ma Q, Liu Y, Su YW, Hwang KC. Post-Buckling Analysis of Curved Beams. *J Appl Mech-T ASME*. 2017; 84:031007.
- Gibson LJ, Ashby MF. *Cellular Solids: Structure and Properties*. Cambridge University Press; 1997.
- Gibson LJ, Ashby MF, Schajer GS. The mechanics of two-dimensional cellular materials. *Proc R Soc Lond A*. 1982; 382:25–42.
- Gonzalez M, Axisa F, BuIcke MV, Brosteaux D, Vandeveld B, Vanfleteren J. Design of metal interconnects for stretchable electronic circuits. *Microelectron Reliab*. 2008; 48:825–832.
- Hasanyan AD, Waas AM. Micropolar Constitutive Relations for Cellular Solids. *J Appl Mech-T ASME*. 2016; 83:041001.
- Huyghe B, Rogier H, Vanfleteren J, Axisa F. Design and Manufacturing of Stretchable High-Frequency Interconnects. *Ieee T Adv Packaging*. 2008; 31:802–808.
- Jang KI, Chung HU, Xu S, Lee CH, Luan HW, Jeong J, Cheng HY, Kim GT, Han SY, Lee JW, Kim J, Cho M, Miao FX, Yang YY, Jung HN, Flavin M, Liu H, Kong GW, Yu KJ, Rhee SI, Chung J, Kim B, Kwak JW, Yun MH, Kim JY, Song YM, Paik U, Zhang YH, Huang Y, Rogers JA. Soft network composite materials with deterministic and bio-inspired designs. *Nat Commun*. 2015; 6:6566. [PubMed: 25782446]
- Jang KI, Jung HN, Lee JW, Xu S, Liu YH, Ma YJ, Jeong JW, Song YM, Kim J, Kim BH, Banks A, Kwak JW, Yang YY, Shi DW, Wei ZJ, Feng X, Paik U, Huang YG, Ghaffari R, Rogers JA. Ferromagnetic, Folded Electrode Composite as a Soft Interface to the Skin for Long-Term Electrophysiological Recording. *Adv Funct Mater*. 2016; 26:7281–7290. [PubMed: 28413376]
- Jones J, Lacour SP, Wagner S, Suo ZG. Stretchable wavy metal interconnects. *J Vac Sci Technol A*. 2004; 22:1723–1725.
- Kang SK, Murphy RKJ, Hwang SW, Lee SM, Harburg DV, Krueger NA, Shin JH, Gamble P, Cheng HY, Yu S, Liu ZJ, McCall JG, Stephen M, Ying HZ, Kim J, Park G, Webb RC, Lee CH, Chung SJ,

- Wie DS, Gujar AD, Vemulapalli B, Kim AH, Lee KM, Cheng JJ, Huang YG, Lee SH, Braun PV, Ray WZ, Rogers JA. Bioresorbable silicon electronic sensors for the brain. *Nature*. 2016; 530:71–76. [PubMed: 26779949]
- Khang DY, Jiang HQ, Huang Y, Rogers JA. A stretchable form of single-crystal silicon for high-performance electronics on rubber substrates. *Science*. 2006; 311:208–212. [PubMed: 16357225]
- Kim DH, Lu NS, Ghaffari R, Kim YS, Lee SP, Xu LZ, Wu JA, Kim RH, Song JZ, Liu ZJ, Viveni J, de Graff B, Elolampi B, Mansour M, Slepian MJ, Hwang S, Moss JD, Won SM, Huang YG, Litt B, Rogers JA. Materials for multifunctional balloon catheters with capabilities in cardiac electrophysiological mapping and ablation therapy. *Nat Mater*. 2011a; 10:316–323. [PubMed: 21378969]
- Kim DH, Lu NS, Ma R, Kim YS, Kim RH, Wang SD, Wu J, Won SM, Tao H, Islam A, Yu KJ, Kim TI, Chowdhury R, Ying M, Xu LZ, Li M, Chung HJ, Keum H, McCormick M, Liu P, Zhang YW, Omenetto FG, Huang YG, Coleman T, Rogers JA. Epidermal Electronics. *Science*. 2011b; 333:838–843. [PubMed: 21836009]
- Klinker L, Lee S, Work J, Wright J, Ma Y, Ptaszek L, Webb RC, Liu C, Sheth N, Mansour M, Rogers JA, Huang Y, Chen H, Ghaffari R. Balloon catheters with integrated stretchable electronics for electrical stimulation, ablation and blood flow monitoring. *Extreme Mech Lett*. 2015; 3:45–54.
- Ko HC, Stoykovich MP, Song JZ, Malyarchuk V, Choi WM, Yu CJ, Geddes JB, Xiao JL, Wang SD, Huang YG, Rogers JA. A hemispherical electronic eye camera based on compressible silicon optoelectronics. *Nature*. 2008; 454:748–753. [PubMed: 18685704]
- Koh A, Kang D, Xue Y, Lee S, Pielak RM, Kim J, Hwang T, Min S, Banks A, Bastien P, Manco MC, Wang L, Ammann KR, Jang KI, Won P, Han S, Ghaffari R, Paik U, Slepian MJ, Balooch G, Huang YG, Rogers JA. A soft, wearable microfluidic device for the capture, storage, and colorimetric sensing of sweat. *Sci Transl Med*. 2016; 8:366ra165.
- Lacour SP, Jones J, Wagner S, Li T, Suo ZG. Stretchable interconnects for elastic electronic surfaces. *P IEEE*. 2005; 93:1459–1467.
- Lee SP, Klinker LE, Ptaszek L, Work J, Liu C, Quivara F, Webb C, Dagdeviren C, Wright JA, Ruskin JN, Slepian M, Huang Y, Mansour M, Rogers JA, Ghaffari R. Catheter-Based Systems With Integrated Stretchable Sensors and Conductors in Cardiac Electrophysiology. *P IEEE*. 2015; 103:682–689.
- Lee YK, Jang KI, Ma YJ, Koh A, Chen H, Jung HN, Kim Y, Kwak JW, Wang L, Xue YG, Yang YY, Tian WL, Jiang Y, Zhang YH, Feng X, Huang YG, Rogers JA. Chemical Sensing Systems that Utilize Soft Electronics on Thin Elastomeric Substrates with Open Cellular Designs. *Adv Funct Mater*. 2017; 27:1605476.
- Li HC, Xu Y, Li XM, Chen Y, Jiang Y, Zhang CX, Lu BW, Wang J, Ma YJ, Chen YH, Huang Y, Ding MQ, Su HH, Song GF, Luo Y, Feng X. Epidermal Inorganic Optoelectronics for Blood Oxygen Measurement. *Adv Healthc Mater*. 2017a; 6:1601013.
- Li Y, Zhang J, Xing Y, Song J. Thermo-mechanical analysis of epidermal electronic devices integrated with human skin. *J Appl Mech-T ASME*. 2017b accepted.
- Liu LP, Lu NS. Variational formulations, instabilities and critical loadings of space curved beams. *Int J Solids Struct*. 2016; 87:48–60.
- Lu BW, Chen Y, Ou DP, Chen H, Diao LW, Zhang W, Zheng J, Ma WG, Sun LZ, Feng X. Ultra-flexible Piezoelectric Devices Integrated with Heart to Harvest the Biomechanical Energy. *Sci Rep-Uk*. 2015; 5
- Lu NS, Yang SX. Mechanics for stretchable sensors. *Curr Opin Solid St M*. 2015; 19:149–159.
- Ma Q, Cheng HY, Jang KI, Luan HW, Hwang KC, Rogers JA, Huang YG, Zhang YH. A nonlinear mechanics model of bio-inspired hierarchical lattice materials consisting of horseshoe microstructures. *J Mech Phys Solids*. 2016a; 90:179–202. [PubMed: 27087704]
- Ma Q, Zhang YH. Mechanics of Fractal-Inspired Horseshoe Microstructures for Applications in Stretchable Electronics. *J Appl Mech-T ASME*. 2016; 83:111008.
- Ma YJ, Feng X, Rogers JA, Huang YG, Zhang YH. Design and application of ‘J-shaped’ stress-strain behavior in stretchable electronics: a review. *Lab Chip*. 2017; 17:1689–1704. [PubMed: 28470286]

- Ma YJ, Jang KI, Wang L, Jung HN, Kwak JW, Xue YG, Chen H, Yang YY, Shi DW, Feng X, Rogers JA, Huang YG. Design of Strain-Limiting Substrate Materials for Stretchable and Flexible Electronics. *Adv Funct Mater.* 2016b; 26:5345–5351. [PubMed: 29033714]
- Mihai LA, Goriely A. Finite deformation effects in cellular structures with hyperelastic cell walls. *Int J Solids Struct.* 2015; 53:107–128.
- Mihai LA, Wyatt H, Goriely A. A Microstructure-Based Hyperelastic Model for Open-Cell Solids. *Siam J Appl Math.* 2017; 77:1397–1416.
- Mooney M. A theory of large elastic deformation. *J Appl Phys.* 1940; 11:582–592.
- Mora RJ, Waas AM. Evaluation of the Micropolar elasticity constants for honeycombs. *Acta Mech.* 2007; 192:1–16.
- Okumura D, Ohno N, Noguchi H. Elastoplastic microscopic bifurcation and post-bifurcation behavior of periodic cellular solids. *J Mech Phys Solids.* 2004; 52:641–666.
- Rogers JA, Someya T, Huang YG. Materials and Mechanics for Stretchable Electronics. *Science.* 2010; 327:1603–1607. [PubMed: 20339064]
- Song J. Mechanics of stretchable electronics. *Curr Opin Solid St M.* 2015; 19:160–170.
- Su YW, Wu J, Fan ZC, Hwang KC, Song JZ, Huang YG, Rogers JA. Postbuckling analysis and its application to stretchable electronics. *J Mech Phys Solids.* 2012; 60:487–508.
- Wang A, Avila R, Ma Y. Mechanics Design for Buckling of Thin Ribbons on an Elastomeric Substrate Without Material Failure. *J Appl Mech-T ASME.* 2017; 84:094501.
- Webb RC, Ma Y, Krishnan S, Li Y, Yoon S, Guo X, Feng X, Shi Y, Seidel M, Cho NH, Kurniawan J, Ahad J, Sheth N, Kim J, Taylor JGt, Darlington T, Chang K, Huang W, Ayers J, Gruebele A, Pielak RM, Slepian MJ, Huang Y, Gorbach AM, Rogers JA. Epidermal devices for noninvasive, precise, and continuous mapping of macrovascular and microvascular blood flow. *Science advances.* 2015; 1:e1500701. [PubMed: 26601309]
- Xu LZ, Gutbrod SR, Bonifas AP, Su YW, Sulkin MS, Lu NS, Chung HJ, Jang KI, Liu ZJ, Ying M, Lu C, Webb RC, Kim JS, Laughner JI, Cheng HY, Liu YH, Ameen A, Jeong JW, Kim GT, Huang YG, Efimov IR, Rogers JA. 3D multifunctional integumentary membranes for spatiotemporal cardiac measurements and stimulation across the entire epicardium. *Nat Commun.* 2014; 5
- Xu LZ, Gutbrod SR, Ma YJ, Petrossians A, Liu YH, Webb RC, Fan JA, Yang ZJ, Xu RX, Whalen JJ, Weiland JD, Huang YG, Efimov IR, Rogers JA. Materials and Fractal Designs for 3D Multifunctional Integumentary Membranes with Capabilities in Cardiac Electrotherapy. *Adv Mater.* 2015; 27:1731–1737. [PubMed: 25641076]
- Xu RX, Lee JW, Pan TS, Ma SY, Wang JY, Han JH, Ma YJ, Rogers JA, Huang YG. Designing Thin, Ultrastretchable Electronics with Stacked Circuits and Elastomeric Encapsulation Materials. *Adv Funct Mater.* 2017; 27:1604545. [PubMed: 29046624]
- Yang SX, Qiao ST, Lu NS. Elasticity Solutions to Nonbuckling Serpentine Ribbons. *J Appl Mech-T ASME.* 2017; 84:021004.
- Zhang P, Parnell W. Band Gap Formation and Tunability in Stretchable Serpentine Interconnects. *J Appl Mech-T ASME.* 2017; 84:091007.
- Zhang RR, Lubin JA, Kuo JS. Bioresorbable Silicon Electronic Sensors for the Brain. *Neurosurgery.* 2016; 79:N19–N19.
- Zhang YH, Huang YG, Rogers JA. Mechanics of stretchable batteries and supercapacitors. *Curr Opin Solid St M.* 2015; 19:190–199.
- Zhu HX. Size-dependent elastic properties of micro- and nano-honeycombs. *J Mech Phys Solids.* 2010; 58:696–709.

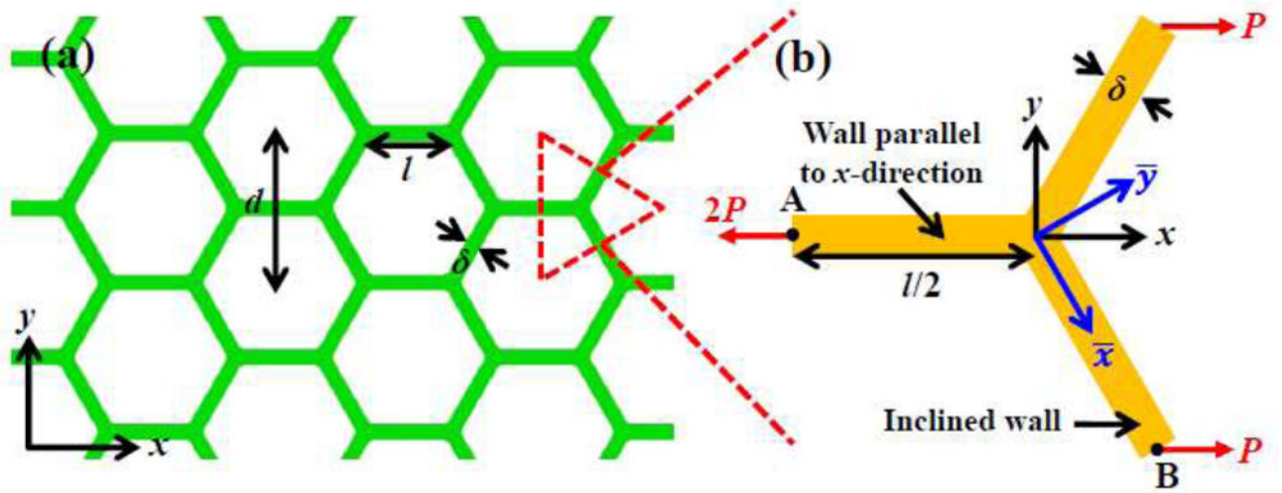


**Figure 1.**  
**(a)** Schematic illustration of cellular substrate, and **(b)** mechanics model of a unit cell.

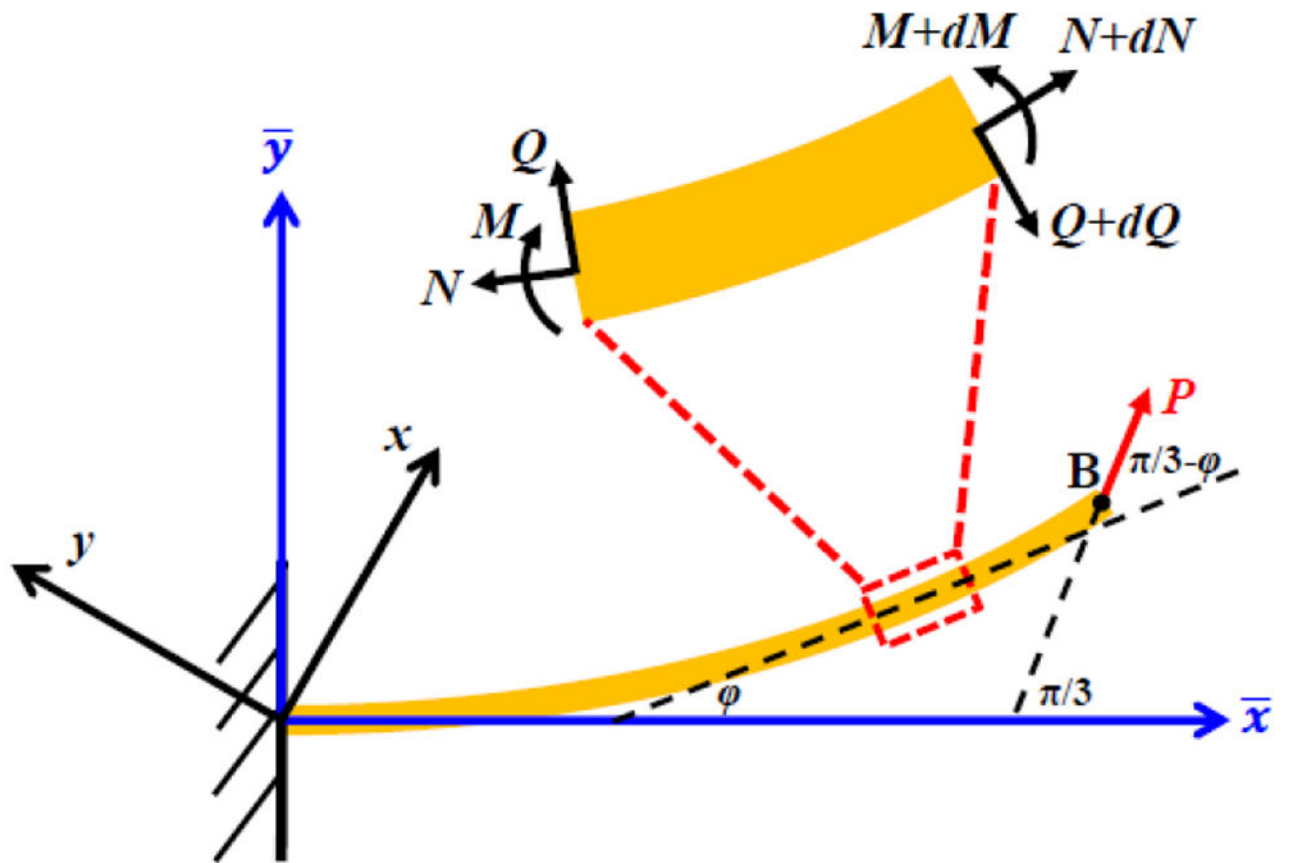


**Figure 2.** Beam model for the inclined cell wall under finite deformation, and the global and local coordinate systems.

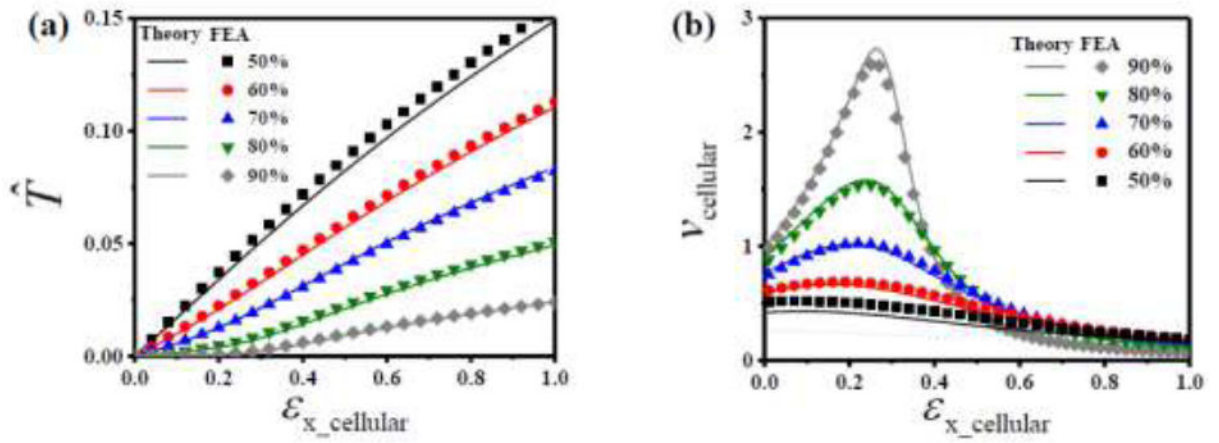


**Figure 3.**

(a) Normalized equivalent nominal stress ( $\bar{T}$ ) and (b) equivalent Poisson's ratio ( $\nu_{cellular}$ ) versus equivalent engineering strain ( $\epsilon_{x\_cellular}$ ) of the equivalent medium for the cellular substrate, obtained by FEA and beam model at different porosities  $\phi = 50\%$ ,  $60\%$ ,  $70\%$ ,  $80\%$  and  $90\%$ .

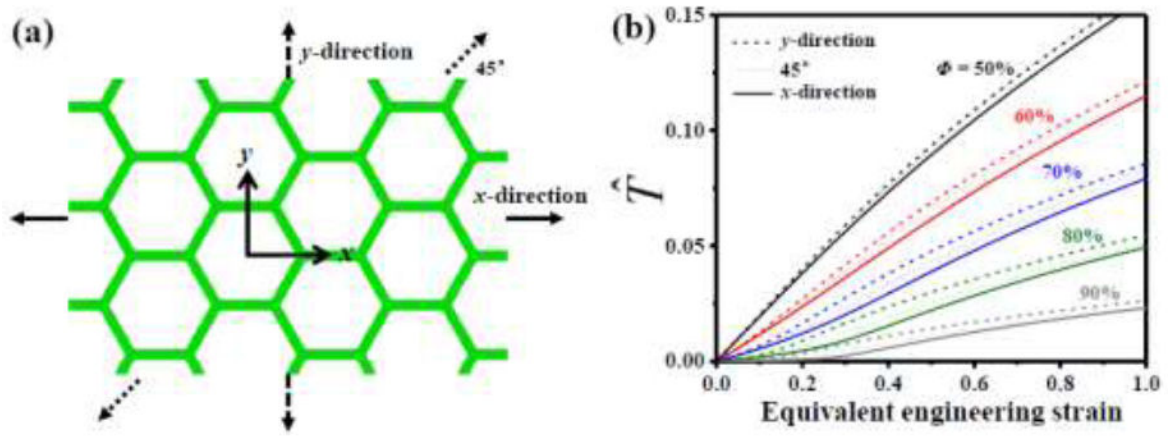


**Figure 4.** Normalized equivalent nominal stress ( $\hat{T}$ ) versus equivalent engineering strain of the equivalent medium for the cellular substrate, obtained by FEA, for different stretch directions ( $x$ -,  $45^\circ$  and  $y$ -directions) and different porosities ( $\phi= 50\%$ ,  $60\%$ ,  $70\%$ ,  $80\%$  and  $90\%$ ).

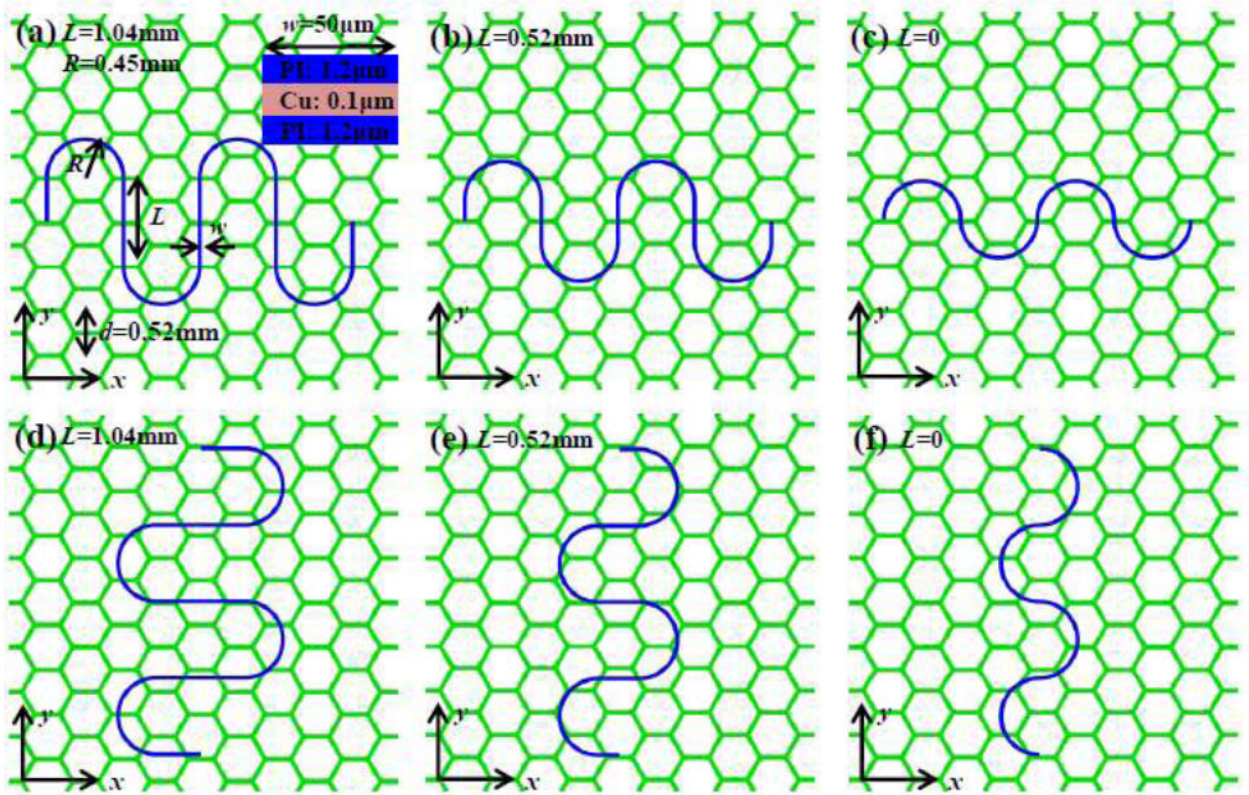


**Figure 5.** Three representative shapes of the serpentine interconnects, with different lengths of the straight part, bonded to the cellular substrate along (a-c)  $x$ - and (d-f)  $y$ -directions, respectively.



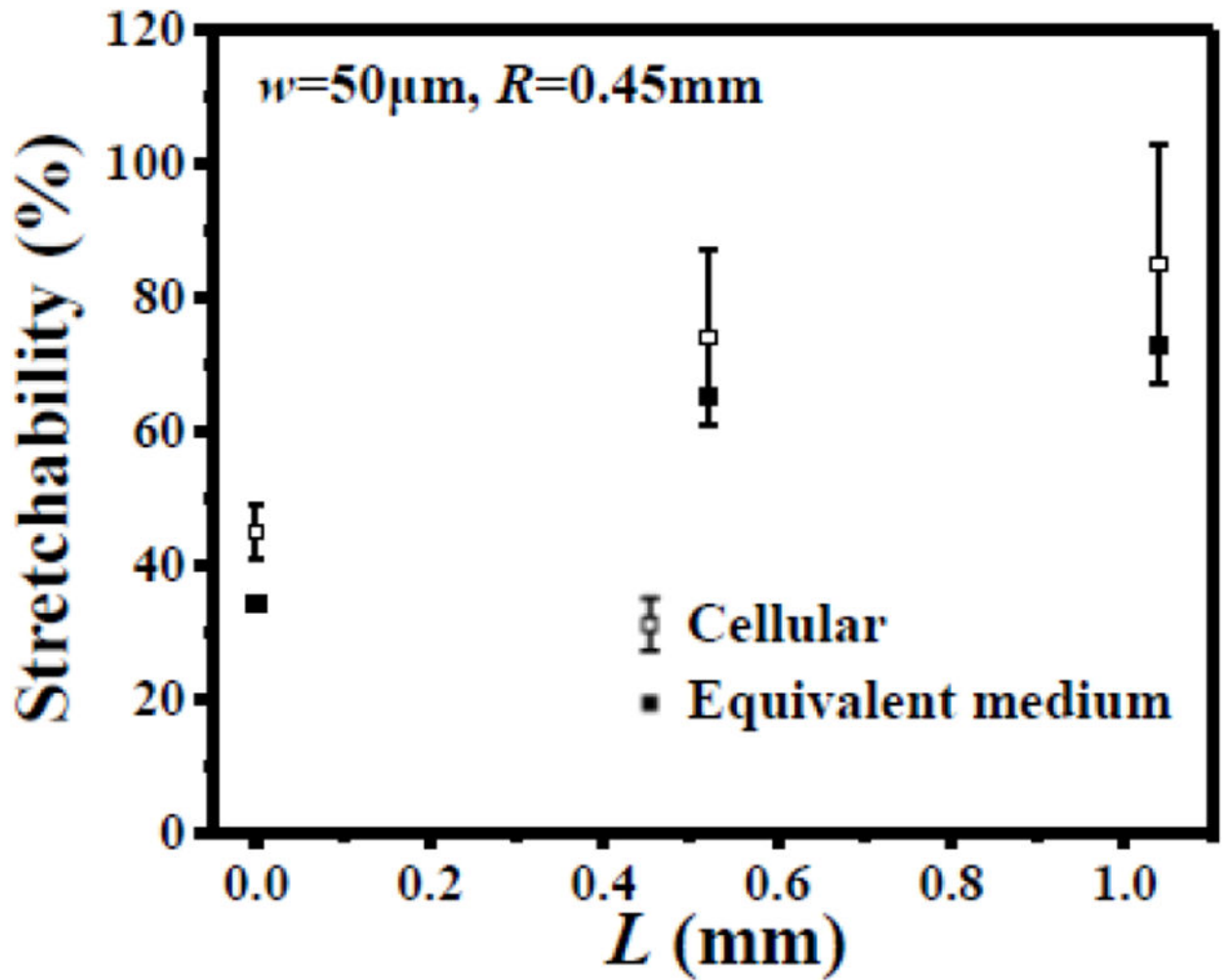


**Figure 6.**

The elastic stretchability of the serpentine interconnect bonded to a cellular substrate, which has a large range of variation due to different alignments, positions and directions of the interconnect on the substrate. The elastic stretchability of the serpentine interconnect bonded to the equivalent medium of the cellular substrate is also shown. Three lengths of the straight part of the serpentine interconnect are taken,  $L = 1.04\text{mm}$ ,  $0.52\text{mm}$  and  $0$ .

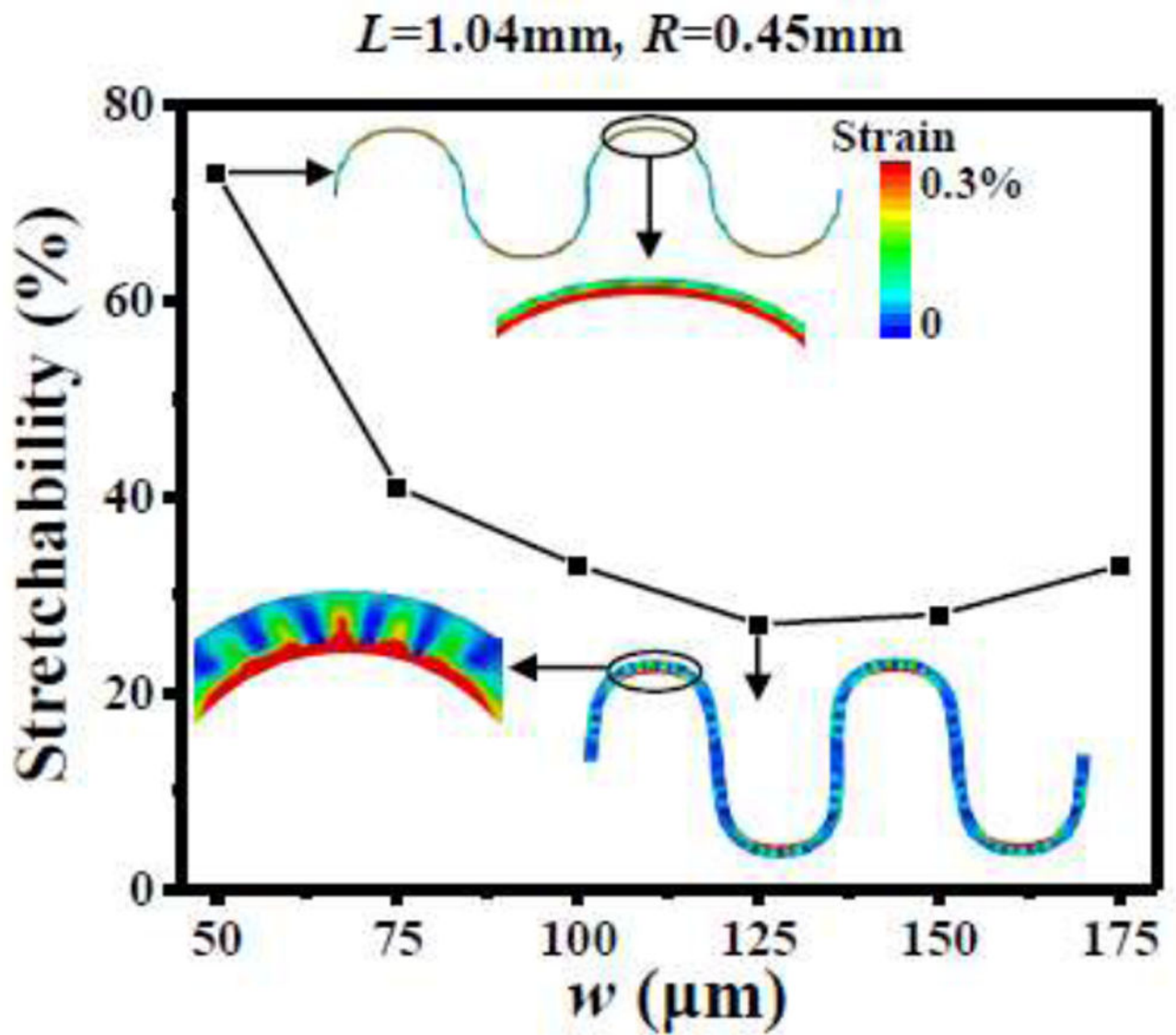


**Figure 7.** The elastic stretchability of the serpentine interconnect, bonded to the equivalent medium of the cellular substrate, versus the interconnect width  $w$  for the fixed length of the straight part  $L = 1.04\text{mm}$  and radius of the circular part  $R = 0.45\text{mm}$ .

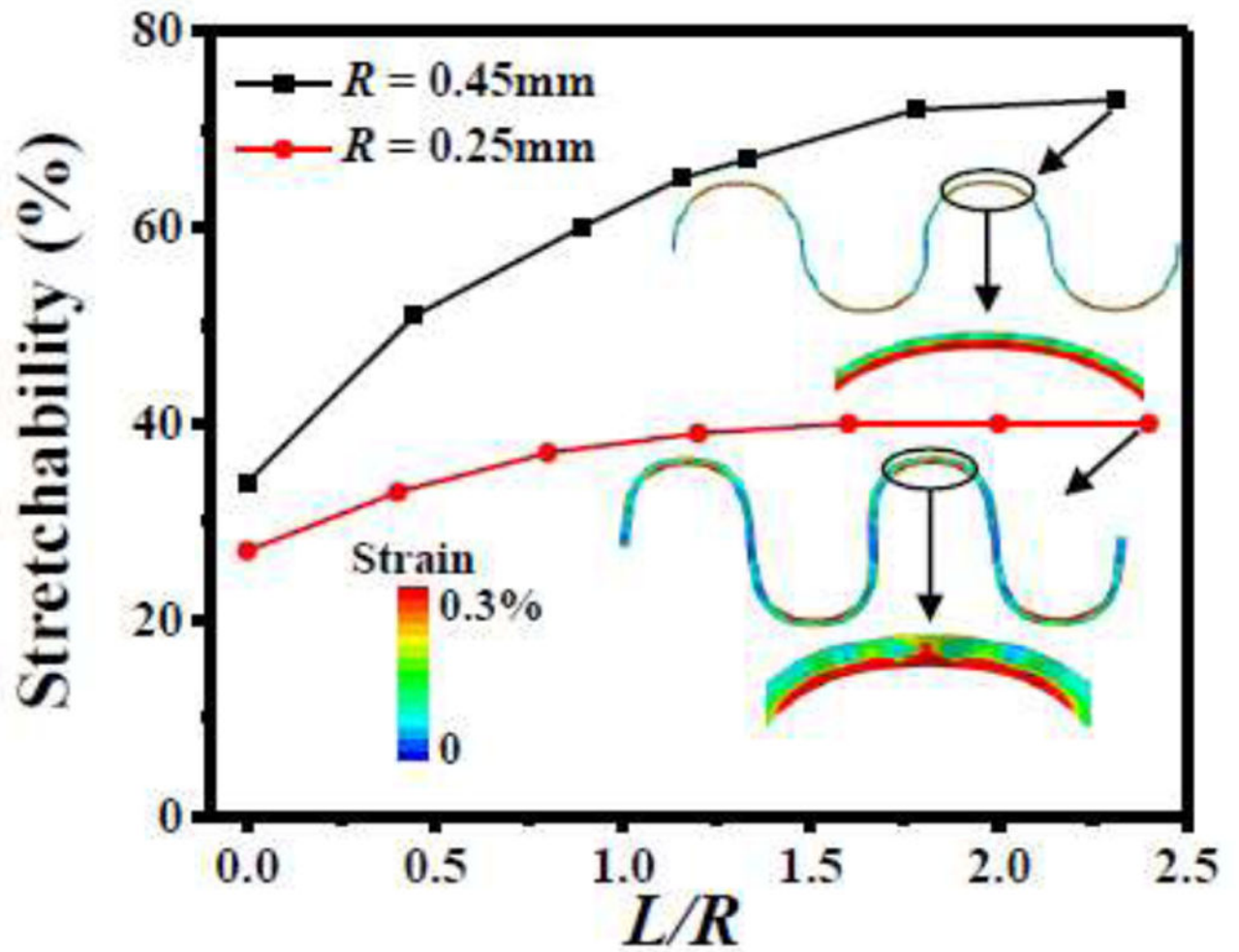


**Figure 8.** The elastic stretchability of the serpentine interconnect, bonded to the equivalent medium of the cellular substrate, versus the length-to-radius ratio  $L/R$  of the serpentine interconnect for the fixed width and  $w = 50\ \mu\text{m}$  and two radii  $R = 0.45\text{mm}$  and  $0.25\text{mm}$ .